Modeling of Thermoelectric Effects in Planar Micromachined Structures Using SPICE

Veljko Milanovi*,* Matthew Hopcroft,‡ Christian A. Zincke,† Mona Zaghloul,† Kristofer S. J. Pister*

Abstract **– This paper presents an improved model for SPICE-based simulation of thermoelectric structures which includes circuit elements for simulating thermoelectric Peltier and Thomson effects, and shows greatly improved accuracy over previous models where those are neglected. The complete thermoelectric model is verified by comparing with experimental results on temperature distributions of suspended aluminum and polysilicon resistors and contacts. Near the contacts, temperature differences of up to 10% of hottest temperature are found when changing current direction. This is closely matched in the presented simulations.**

I. INTRODUCTION

Recent advancements in micromachining and microelectromechanical systems (MEMS) have brought about a new *genre* of miniature thermoelectric devices for a variety of applications. A new class of thermoelectric devices has been demonstrated recently in CMOS MEMS processes [1],[2], whereby post-processing micromachining of CMOS yields efficient thermal and electromagnetic structures. These devices include thermocouple-based ac-dc thermoconverters [3],[4], microwave power sensors [5], chemical sensors [6], infrared emitters and detectors, and even accelerometers [7].

The design and characterization of these thermoelectric structures demands an understanding of the various thermoelectric effects present in the device and a simulation environment suitable for modeling these effects. Such simulations have been performed by different numerical methods. Another methodology, first proposed by Potter [8] is to make use of the analogies between the electrical and thermal domains and use an electrical simulation tool, such as SPICE, to perform thermal simulations. Others have utilized this methodology recently in different applications [9]-[15]. One advantage of such an approach is the simplicity, as well as taking advantage of present simulation tools. Another important benefit for the above mentioned new *genre* of thermoelectric devices is that both the electric and thermal phenomena can be simulated simultaneously in a common, already available tool, thereby simplifying simulation of overall device performance.

Previous approaches neglected thermoelectric Peltier and Thomson effects, which result in second-order temperature changes and can in some cases have very little overall effect. In other cases, however, temperature distribution discrepancies of up to 10% are found between first-order model predictions and experimental results. Finally, there are applications such as thermoelectric coolers where the very principle of operation is based on the thermoelectric effects. The accuracy of the simulations could be greatly improved by including these, particularly in thermoconverter and cooler applications where these are essential in determining specifications.

*Berkeley Sensor and Actuator Center, University of California at Berkeley, 497 Cory Hall #1770, Berkeley, CA 94720-1770 veljko@eecs.berkeley.edu.

‡Analatom, Incorporated, of Sunnyvale, CA.

†Dept. of Electrical and Computer Engineering, The George Washington University, Washington, DC 20052.

The work was partially supported by SPAWAR Sys. Cen., RDT&E DIV, San Diego, CA.

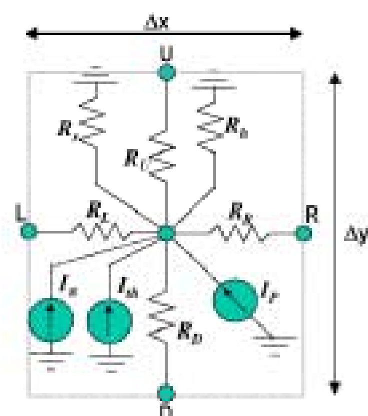

Figure 1. Equivalent electrical circuit representation of an element including convection, conduction, radiation, and heat generation, as well as Peltier and Thomson current sources.

In this work, we present an improved SPICE model for thermoelectric simulation of planar micromachined structures which includes both the Peltier and Thomson effects. The model is applied on two simple test structures which were fabricated and characterized using a thermal microscope. Results from the model are shown to be in close agreement with experimental results for the two structures under varied applied voltage conditions.

II. SPICE EQUIVALENT CIRCUIT FOR THERMAL MODEL

In the work of Swart and Nathan [10], the thermal conduction, radiation, and convection equations are translated into equivalent voltage controlled current source (VCCS) circuit elements and subsequently solved using SPICE. The following nomenclature is used in this work, in agreement to that in [10]:

- A Area (m^2)
- h Heat-transfer coefficient (W/m^2K)
- I Current (A)
- l Length (m)
- q Heat transfer/unit area (W/m^2)
- α Seebeck coefficient
- π_{ab} Peltier coefficient between materials a and b
- γ_{th} Thomson coefficient
- T Temperature (K or °C)
- t_{CR} Temperature coefficient of resistance (1/K)
- κ Thermal conductivity (W/mK)
- T Absolute temperature (K)
- V Voltage (V)
- R_0 Resistance at room temperature (Ω)

Heat flow is represented as current, temperature as voltage, and heat power as electrical power. Our application of the methodology to thermoelectric power sensors [15] details the simulation setup. In short, the two-dimensional micromachined thermoelectric structure is subdivided into small elements within each material, as for finite difference type of numerical simulation. In place of each structural element, a representative electrical circuit is inserted as given in Fig. 1. The circuit

includes four non-linear resistor elements to represent thermal conduction (R_L,R_R,R_D,R_U), a non-linear resistor to represent thermal convection (R_h), a non-linear resistor to represent radiation (R_r) and a non-linear current source (I_P) to represent Joule heat generation. The current source I_P in Fig. 1 is only applicable for resistive elements in the device structure where dissipated power generates heat, and may also have temperature and other dependence. The figure also shows two additional current sources, I_π and I_{th} , representing thermoelectric effects, which will be discussed in detail in Section III, and have not been included in past models.

Each of these circuit elements is generally a polynomial VCCS due to temperature (represented as voltage) dependence of most material properties. The form used here is:

$$I = a_0 + a_1 V + a_2 V^2 + \dots . \quad (1)$$

Since the test structures are designed for operation <200 °C, radiation effects can be included into the same linear resistor term with convection. This is only used for simplification, while the model clearly allows for a T^4 dependence by applying the appropriate coefficients for the radiation circuit element.

Only the steady state temperature solutions are of interest, so thermal conduction equation is given by:

$$\nabla \cdot (\kappa \nabla T) = -I_{el}^2 R_0 (1 + t_{CR}(T - T_0)) - h(T - T_0) . \quad (2)$$

The first term on the right hand side of (2) represents Joule heating of the element due to electrical current I_{el}. The thermistor effect in the given material is represented by the temperature coefficient of resistance, t_{CR}. The second term on the right hand side represents the heat losses due to convection.

The thermal conduction in the left hand side of (2) is represented by resistors R_L,R_R,R_D,R_U, as mentioned before. In the simple case where there is no variation in material thermal parameters due to change in temperature:

$$R_{L,R,D,U} = \frac{l_{L,R,D,U}}{\kappa \cdot A} , \quad (3)$$

where A is cross-sectional area of the element, and l is determined by the segmentation of the structure, such that l_L=l_R=$\Delta x/2$, and l_D=l_U=$\Delta y/2$. This assigns the coefficients of the VCCS in (1) with a_1=κA, and a_0=0 and sets up the four conduction resistors which differ from element to element by κ and A. The convection resistor R_h is also represented by a VCCS with a_1=hA to implement (2), but here A is surface area in the plane of the wafer. Joule heat generation, equal to power dissipation, could be modeled by a constant-current source. However, as mentioned above the input power in many structures, particularly in CMOS MEMS, is dissipated by the thin-film polysilicon heater, whose resistance is a strong function of temperature. Therefore, the input power is implemented as:

$$I_P(T) = I_{el}^2 R_0 + I_{el}^2 R_0 \cdot t_{CR}(T - T_0), \quad (4)$$

which sets up a_0=$I^2 R_0$ and a_1=t_{CR} $I^2 R_0$

Our analysis in this work is simplified from [10] in the following ways. In the convection model, only natural convection is of interest, and all convective losses are lumped into one thermal resistance term. An additional simplification is that the temperature dependence of thermal conductivity for the materials present is neglected.

III. Thermoelectric Effects

The basic model described in the previous section does not account for the thermoelectric Peltier, Thomson, and Seebeck effects [17]. These effects occur due to the temperature dependence of the Fermi level in a material, and to some extent affect all materials and all junctions between any two dissimilar materials. Peltier and Thomson effects cause redistribution of heat and hence cause a different temperature distribution from that predicted by the solution of (2). For this reason, the effects need be included in the model. On the other hand, the Seebeck effect, which is related to the other two, does not result in a different solution of temperature but instead affects electric potentials, and is therefore not directly relevant in this model.

A. The Peltier Effect

The Peltier effect [17] is related to electrical current and temperature at a junction of two dissimilar materials. When a current flows through a junction of two different conductors, heat is either absorbed or released, the effect depending on the direction of the current flow. The rate of absorbed or released Peltier heat q_p is proportional to the current flow I_{el} and the relative Peltier coefficient π_{ab}:

$$q_\pi = \pi_{ab}(T) \cdot I_{el_ab} , \quad (5)$$

where I_{el_ab} is passing from material a to material b. The first Kelvin relation relates the Peltier coefficient with the Seebeck coefficient as [17]:

$$\pi_{ab}(T) = \alpha_{ab} \cdot T . \quad (6)$$

In a thermoconverter application, the Peltier effect can, at higher currents (e.g. power measurement above 1 mW,) result in significant deviation from linearity. In high frequency applications, the Peltier heat changes sign much faster than the thermal time constant of the system and the effect is therefore canceled. The problem still exists in any such sensors that utilize dc calibration, bias, or reference.

The proposed model accounts for the Peltier heating and cooling at the junctions by introducing current sources at circuit nodes corresponding to the contacts. The current source is shown in Fig. 1 and is only applicable for elements corresponding to material junctions. These current sources are given by:

$$I_\pi = \pi_{ab} \cdot I_{el_ab} = V \cdot \alpha_{ab} \cdot I_{el_ab} , \quad (7)$$

i.e. a VCCS with only one coefficient, a_1=$\alpha_{ab} I_{el_ab}$, is introduced. It should be noted that the value of the current I_{el_ab} that is used in the coefficient corresponds to the portion of the overall current that flows through that very element. This assumes uniform current distribution through the resistor which is not true in general, and is not a necessary assumption.

B. The Thomson Effect

Thomson effect arises in bulk material due to the temperature dependence of the Seebeck coefficient [17]. When a temperature difference, ΔT, is present along a conductor of finite resistance in which a current flow causes the generation of Joule heat, an additional amount of heat q_{th} is absorbed from or released depending on the relative direction of the current flow and the temperature gradient direction. The Thomson heat generation or absorption rate q_{th} is defined as:

$$q_{th} = \gamma_{th}(T) \cdot \vec{I}_{el} \cdot \vec{\nabla} T , \quad (8)$$

where γ_{th} denotes the Thomson coefficient. The second Kelvin relation connects the Seebeck effect with the Thomson effect as:

$$\gamma_{th} = T \frac{\partial \alpha(T)}{\partial T} . \quad (9)$$

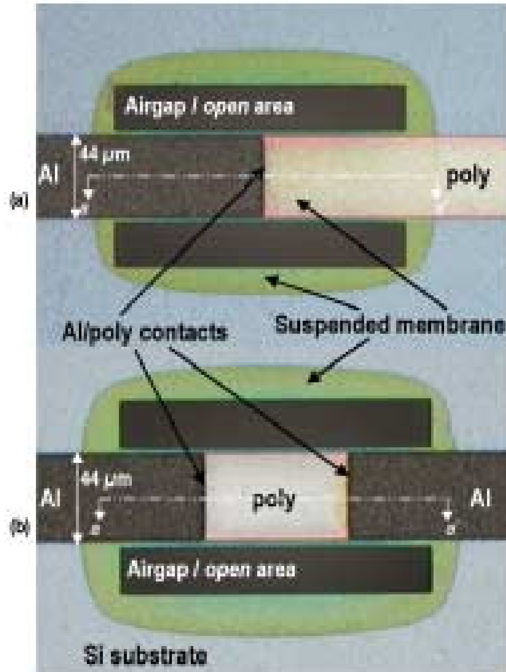

Figure 2. Test structures for thermoelectric effect modeling and measurement (a) single metal-polysilicon contact bridge, and (b) double contact metal-polysilicon bridge.

Because the heat generation is proportional to the dot product of the temperature gradient to electrical current, the model element is a current source with dependence on different voltages from neighboring nodes. Namely, if e.g. current was flowing from node L to node R in Fig. 1, knowledge of temperature at both nodes and the center node is required. To simplify implementation of eqs. (8) and (9), we utilized the "*B*" command in SPICE 3.0 which allows for an arbitrary function statement. The command for element I_{th} of Fig. 1 is:

Bth 0 center I=v(center)*C*(v(L)-v(R)),

where $C = I_{el} \dfrac{\partial \alpha(T)}{\partial T}$

III. Fabrication and Measurement Setup

The test structures were fabricated at the Berkeley Microfabrication Facility in a CMOS-compatible process that included only polysilicon, aluminum, and dielectric layers for the purpose of fabricating the thermoelectric test structures.

Backside etching was then used to remove the bulk silicon substrate from beneath the thermoelectric test structures and achieve thermal isolation. Examples of fully fabricated devices are shown in Fig. 2. The device in Fig. 2a is a suspended membrane encapsulating an aluminum resistor in contact with a polysilicon resistor. The structure in Fig. 2b includes two such Al-poly contacts and is structurally symmetric. Its aim is to characterize the asymmetry of temperature distribution due to both thermoelectric effects.

Thermal measurements of the test structures were performed using a thermal imaging microscope with a temperature-controlled stage. Suspended test structures were packaged in 40-pin DIP and mounted on a copper block attached to the microscope stage. Power was applied to the devices using a

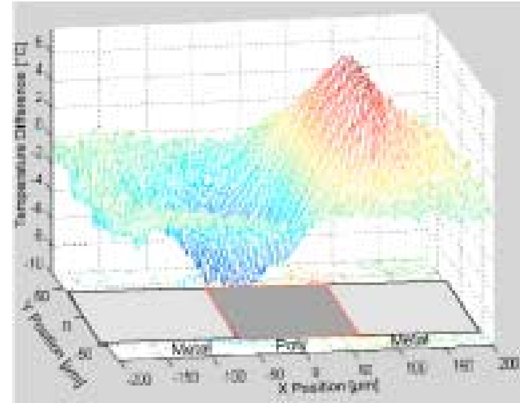

Figure 3. Difference of measured temperature distributions for structure in Fig. 2b with positive dc applied and negative dc applied at same power 10 mW.

variable voltage source in three ways: positive dc voltage, negative dc voltage, and ac voltage. Care was taken to apply same power under all three conditions, to obtain a good comparison of temperature distributions.

The thermal imaging microscope records 2-D images of radiance in the infrared wavelength range. Before the measurements were taken, the inherent radiance of the chip was recorded. This data was used by the microscope to compensate for the inherent radiance of the device. A zero-input radiance image was used to align the thermal images with the actual devices. Temperature distributions obtained from the same device under three applied power conditions were compared. Figure 3 shows the difference between two obtained temperature distributions for the structure in Fig. 2b under positive and negative dc applied. This result is a good example of large temperature discrepancies of >10% of maximum temperature at contacts that cannot be predicted by previous models.

IV. Simulation Results and Discussion

The three-dimensional structure of either device in Fig. 2 is treated as 2D in the layout plane, due to the fact that only air is present above and below the structure, and the convective losses in those directions can be combined into one resistive circuit element at each element in the plane. The 2D layout is further subdivided into smaller elements, each being one of three types (encapsulated polysilicon, encapsulated metal, membrane). Elements of $\Delta x=2\ \mu m$ and $\Delta y=2\ \mu m$ were used. Each element is then represented as the equivalent circuit of Fig. 4, with particular values depending on the element type, and size.

Simulations were set up by forcing constant current excitation I_{el} through resistor, therefore nominally forcing input power $(I_{el})^2 R_{term}$. The even symmetry condition across the cuts a-a', as outlined in Fig. 2, was set up by doubling values of resistors R_L and R_R in the bottom row, and cutting off lower resistors R_D in that same row. The constant input current $I_{el}/2$ was therefore forced into the (half) resistor, which enters (2). After the network of VCCSs is created and simulated in SPICE, the resulting node voltages are treated as temperatures, and the heater temperatures are fed back to obtain the adjusted resistance:

$$R_{term_adj} = R_0 \sum_i \left(1 + \alpha_{poly} \cdot (T_i - T_0)\right), \tag{10}$$

since each *i-th* subdivision has increased resistance. Hence, the

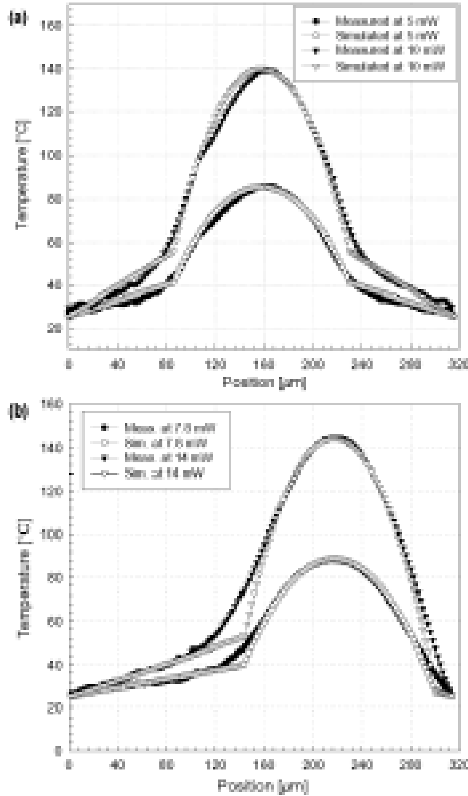

Figure 4. Compared measured and modeled temperature distribution across suspended resistor: (a) device of Fig. 2a at two ac signals applied, 5 mW and 10 mW, (b) device of Fig. 2b for model and measurement at two ac signals applied, 7.8 mW and 14 mW.

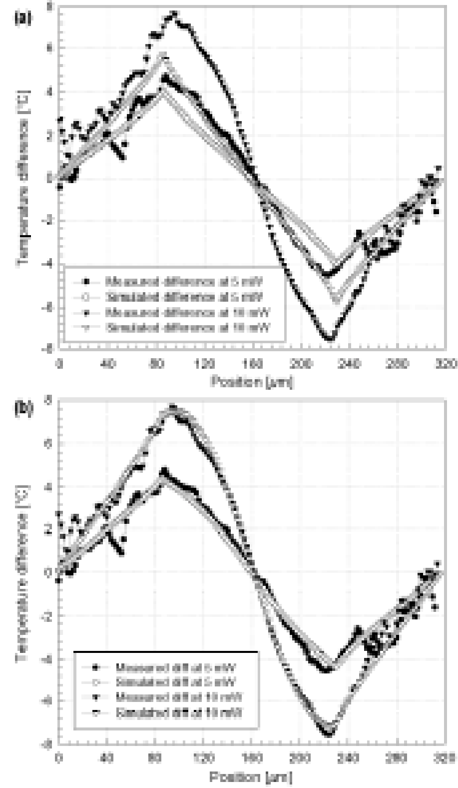

Figure 5. Difference of measurements and difference of simulations for device in Fig. 2b with positive dc applied and negative dc applied at 5 mW and at 10 mW: (a) Peltier effect included in model, (b) complete model with both Peltier and Thomson effects.

actual power dissipated in the termination resistors is:

$$P_{diss} = (2I)^2 \cdot R_{term_adj} \, . \tag{11}$$

After running the SPICE simulations, we identified the nodes that belong to the center cut through the resistor (a-a' in Fig. 2). The modeled results were compared with measured ones also taken from the center cut through resistor thermal image. The comparison of model and simulations for the a-a' cut through the structures of Fig. 2 are shown in Fig. 4 for two applied powers P_{diss}. In the figures, it can be seen that the modeled temperature distribution with convection included closely resembles the measured distribution. At the contacts, due to the limited resolution of the thermal microscope (~10 μm), the measured temperature distribution shows slow transitions from polysilicon to metal. This is likely not the actual temperature profile in that vicinity, but a convolution of the temperature and the microscope's resolution-limited spot size. The measurements and simulations compared in Fig. 4 were done with applied ac signal of 10 kHz, well beyond the thermal response of the device, namely they do not exhibit thermoelectric effects. Similarly, measurements and simulations were done with applied positive and negative dc signal. For comparison, and verification of the model, the measurements were subtracted between the two applied conditions to obtain asymetry from thermoelectric effects, as in Fig. 3. Same was done with simulated temperature distributions in which Peltier effect was included, but not Thomson. This comparison is shown in Fig. 5a. It is evident that

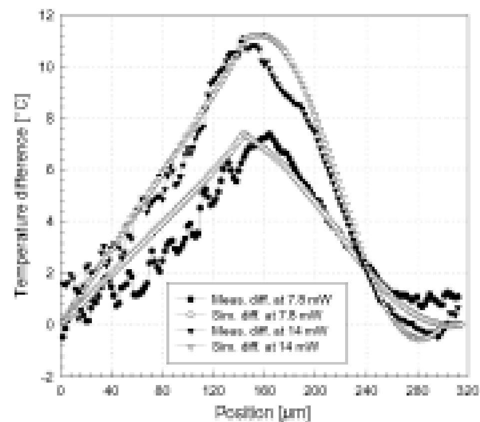

Figure 6. Compared results of temperature distribution across resistor bridge of Fig. 1b for model and measurement at two ac signals applied, 7.8 mW and 14 mW.

the Peltier model alone is not sufficient to accurately model the peak difference value and the *sinusoidal* shape of the difference. With the complete model, including both effects, much better match was observed between measurements and simulation, as given in Fig. 5b and Fig. 6. The data is somewhat noisy since differences of only several degrees are being observed but the trends and the match with model are clear. The benefit of

comparing difference curves is that much of the unwanted smoothing due to microscope's 10 μm spot size is eliminated.

V. Conclusions

The presented modification of thermal SPICE model shows very good performance when applied to measured planar thermoelectric devices. This work completes the previously proposed methodology for thermal modeling using SPICE, such that an integrated, common, tool for coupled electrical and thermal simulation can be created based on present simulators. In the future, more accurate measurements with higher resolution should be utilized to determine the accuracy of the model.

VI. Acknowledgements

The authors are greatful to Michael Gaitan, Jon Geist and Mehmet Ozgur for assistance with thermal measurements and technical discussions, and Chris Keller and Dana Teasdale for assistance with fabrication.

References

[1] N. H. Tea, V. Milanovi', C. Zincke, J. S. Suehle, M. Gaitan, M. Zaghloul, and J. Geist. "Hybrid Post-processing Etching for CMOS-compatible MEMS," *IEEE/ASME Journal of MEMS*, 1997.

[2] H. Baltes, "Future of IC microtransducers," *Sensors and Actuators A (Physical)*, vol. A56, no.1-2, pp.179-192, Aug. 1996.

[3] D. Jaeggi and H. Baltes, "Thermoelectric AC Power Sensor by CMOS Technology," IEEE Electron Device Letters, vol. 13, no. 7, Jul. 1992.

[4] M. Gaitan, J. Kinard, and D. X. Huang, "Performance of Commercial CMOS Foundry-Compatible Multijunction Thermal Converters," Transducers'93 Conf., Yokohama, Japan, Jun. 1993.

[5] V. Milanovi', M. Gaitan, E. Bowen, N. Tea, and M. Zaghloul, "Thermoelectric Power Sensor for Microwave Applications in CMOS Technology," *IEEE Electron Device Lett.*, vol. 18, pp. 450-452, Sep. 1997.

[6] J. S. Suehle, R. E. Cavicchi, M. Gaitan, and S. Semancik, "Tin Oxide Gas Sensor Fabricated Using CMOS Micro-Hotplates and In-Situ Processing," IEEE Electron Device Lett., Vol. 14, No. 3, p. 118, 1993.

[7] V. Milanovi', E. D. Bowen, M. E. Zaghloul, N. H. Tea, J. S. Suehle, B. Payne, M.Gaitan, "Convective Accelerometer and Tilt Sensor in CMOS Technology," Applied Physics Letters, vol. 76, no. 2, Jan. 2000.

[8] N. L. Potter, "Electrical Analogue for Heat Flow Problems in Semiconductors," Electron. Eng., Aug. 1959.

[9] R. Wilson, P.W.R. Scott, R. H. Moult, H. S. Gamble, A.S. Hudson, "A SPICE Based Thermal Model for the Estimation of Peak Current Capability of Thyristor Based Devices,"

[10] N. R. Swart and A. Nathan, "Flow-rate microsensor modelling and optimization using SPICE," Sensors and Actuators A, vol. 34, pp. 109-122, 1992.

[11] H. Sasaki, K. Takahashi, B. D. Inglis, and M. Klonz, "A Numerical Simulation of Thermoelectric Effects in Single-Junction Thermal Converters," *IEEE Trans. On Instrumentation and Measurement*, vol. 48, no. 2, April 1999.

[12] J. R. Kinard, J. R. Hastings, T. E. Lipe, and C. B. Childers, "AC-DC Difference Calibration," NIST Special Publication, May 1989.

[13] D. Moser, R. Lenggenhager, H. Baltes, "Silicon gas flow sensor using industrial CMOS and bipolar IC technology," Sensors and Actuators A, vol. 25-27, pp. 577-581, 1991.

[14] H. B. Callen, Thermodynamics and an Introduction to Thermostatics, 2nd ed., John Wiley & Sons, New York, 1985.

[15] V. Milanovi', M. Hopcroft, C. A. Zincke, M. Gaitan, and M. E. Zaghloul, "Optimization of CMOS MEMS Microwave Power Sensors," Proc. of Int. Symp. on Circuits and Systems - ISCAS'99, vol. V, pp. 144-147, Orlando, FL, Jun. 1999.

[16] Rudolph, H., "Simulation of Thermal Effects in Integrated Circuits with SPICE – A Behavioural Model Approach," *Microelctronics Journal*, vol. 24, No. 8, pp. 849-861, Dec. 1993.

[17] G.C.M. Meijer, A.W. van Herwaarden, *Thermal Sensors*, Institute of Physics Publishing, Great Britain, 1994.